



ELSEVIER

Available online at www.sciencedirect.com

ScienceDirect

Proceedings of the Combustion Institute 31 (2007) 575–583

Proceedings
of the
Combustion
Institute

www.elsevier.com/locate/proci

Detailed kinetic modeling of soot formation in shock tube pyrolysis and oxidation of toluene and *n*-heptane

G.L. Agafonov^b, I. Naydenova^a, P.A. Vlasov^b, J. Warnatz^{a,*}

^a Interdisziplinäres Zentrum für Wissenschaftliches Rechnen (IWR), Universität Heidelberg,
Im Neuenheimer Feld 368, D-69120 Heidelberg, Germany

^b Semenov Institute of Chemical Physics, Russian Academy of Sciences, Kosygin str. 4, 119991 Moscow, Russia

Abstract

A new detailed kinetic model of soot formation in shock tube pyrolysis and oxidation of aliphatic and aromatic hydrocarbons is proposed. The model is based on the comprehensive kinetic model of PAH formation and growth [H. Richter, J.B. Howard, *Phys. Chem. Chem. Phys.* 4 (2002) 2038–2055; H. Richter, S. Granata, W.H. Green, J.B. Howard, *Proc. Combust. Inst.* 30 (2005) 1397–1405; J. Appel, H. Bockhorn, M. Frenklach, *Combust. Flame* 121 (2000) 122–136; M. Frenklach, D.W. Clary, T. Yuan, W.C. Gardiner, Jr., S.E. Stein, *Combust. Sci. Tech.* 50 (1986) 79–115; M. Frenklach, J. Warnatz, *Combust. Sci. Tech.* 51 (1987) 265–283; M.S. Skjøth-Rasmussen, P. Glarborg, M. Østberg, J.T. Johannessen, H. Livbjerg, A.D. Jensen, T.S. Christensen, *Combust. Flame* 136 (2004) 91–128], on the new concepts of soot particle nucleation [A. Violi, *Combust. Flame* 139 (2004) 279–287; A. Violi, A.F. Sarofim, G.A. Voth, *Combust. Sci. Tech.* 176 (2004) 991–1005; A. D'Alessio, A. D'Anna, P. Minutolo, L.A. Sgro, A. Violi, *Proc. Combust. Inst.* 28 (2000) 2547–2554; A. D'Anna, A. Violi, A.D'Alessio, A.F. Sarofim, *Combust. Flame* 127 (2001) 1995–2003] and the traditional H-abstraction/C₂H₂-addition (HACA) route of PAH and soot particles surface growth [H. Wang, M. Frenklach, *Combust. Flame* 110 (1997) 173–221; J. Appel, H. Bockhorn, M. Frenklach, *Combust. Flame* 121 (2000) 122–136]. The gas-phase kinetic scheme was validated against the experimentally measured concentration profiles of the main gas-phase species formed during toluene pyrolysis and H and OH radicals during benzene and phenol pyrolysis and toluene oxidation behind reflected shock waves. The model describes the main characteristics of soot formation in pyrolysis and oxidation of toluene and *n*-heptane oxidation under conditions typical of shock tube experiments. Both hydrocarbons have the same number of carbon atoms but different structures, which causes different behavior of the systems. The discrete Galerkin technique was applied for direct counting of the mean number of active sites formed on the surface of soot precursors and soot particles in reactions of activation, deactivation, and surface growth.

© 2006 The Combustion Institute. Published by Elsevier Inc. All rights reserved.

Keywords: Soot; PAH; Kinetic modeling; Pyrolysis; Oxidation

1. Introduction

Recent progress in development of the chemistry of polycyclic aromatic hydrocarbons (PAHs) [1,15–17] provides foundation for further

* Corresponding author. Fax: +0049 6221 54 8884.
E-mail address: warnatz@iwr.uni-heidelberg.de (J. Warnatz).

improvement of the kinetic models of soot formation. The essence of the models presented in the literature is the increase in particle mass by chemical reactions with gaseous species simultaneously with the growth of particle size by collisions among PAH species. Violi [1] considered two main reaction sequences as possible pathways that contribute to the aromatic growth: the growth of aromatics by a radical–molecule sequence of reactions involving five-member ring PAHs, which are present at large concentrations in the reacting mixture, and the traditional HACA mechanism [2]. In the context of this model [1], soot precursors with different structure are formed in case of benzene and acetylene flames. In contrast to 3D structures formed in aromatic flames, the structures formed in aliphatic flames are instead mainly planar and the contribution of C_2H_2 is significant. These results are in agreement with the findings reported by Homann et al. [3,4]. The C/H ratios experimentally determined in [3] for acetylene flame showed that soot nucleation starts with the formation of PAH structures, while further growth results in the formation of PAHs with unique structures of totally condensed hexagons. In benzene flames [4], a variety of possible PAH structures were observed possessing different C/H ratios. It should be noted that either in benzene or acetylene flames the observed C/H ratios of the hydrocarbon species formed considerably differ from those that would be observed in case of fast polymerization of polyynes. Frenklach and Wang [5,6] introduced the hypothesis of chemical similarity: the surface of soot particles was assumed to look like the edge of large PAH molecules, covered with C–H bonds. Abstraction of these H radicals activates the sites, forming surface radicals. Howard et al. [7,8] described the formation of active sites on PAH molecules as a result of H atom abstraction. These sites provide a chemical basis for reactive coagulation of PAH compounds with each other and with small radicals. Recent experimental findings of Wang et al. [9] confirmed that freshly nucleated soot is made primarily of aromatics. As it was experimentally observed in [9], while soot nucleation and mass growth at the early stage are dominated by aromatics, the reaction of aliphatic species with preexisting soot surface is an important factor at the late stage of soot mass growth.

The main goal of the present work is the development of a kinetic model of soot formation based on the new concepts of PAH formation and growth [7,8,14], soot precursor nucleation [1,15–17], and the traditional surface HACA mechanism of soot particle growth [10]. The gas-phase mechanism of the kinetic model was validated against experimentally measured profiles of the main gas-phase products of toluene pyrolysis [20] and H and OH radical concentrations measured correspondingly during benzene and phenol pyrolysis [21,22] and during oxidation of

toluene and *n*-heptane [23] in shock tube experiments. The model of soot formation developed was applied to simulate soot formation in toluene pyrolysis and oxidation [24] and *n*-heptane rich oxidation [25] in shock tube experiments.

2. Description of the kinetic model

The kinetic model of soot formation developed consists of the gas-phase reaction mechanism, which describes the pyrolysis and oxidation of the parent hydrocarbons, in particular toluene and *n*-heptane, and the formation and growth of PAHs through different reaction pathways up to coronene. The formation, growth, oxidation, and coagulation of soot precursors and soot particles are described within the framework of a discrete Galerkin technique [26].

The gas-phase reaction mechanism is based on the reaction sequence of PAH formation in laminar premixed acetylene and ethylene flames (HACA) [2], with all modifications presented in the work [10]. Several additional channels of PAH formation and growth (up to coronene) [8] and a comprehensive set of reactions of C_3 -, C_5 -, and C_7 -hydrocarbons [7,14] was also added in the kinetic mechanism. Thus, several pathways of PAH formation and growth are incorporated in the reaction mechanism: (1) the alternating H-abstraction/ C_2H_2 -addition (HACA) route, resulting in a successive growth of PAHs, (2) the combination reactions of phenyl with C_6H_6 , (3) the cyclopentadienyl recombination, and (4) the ring closure reactions of aliphatic hydrocarbons. *n*-Heptane oxidation was described within the kinetic scheme presented in [13]. Thus, the modified gas-phase reaction mechanism of the model consists of 2250 direct and reverse reactions between 210 different species, where the rate coefficients of some important reactions have pressure dependence. The main difference of the gas-phase mechanism developed in the present work in comparison with the mechanism proposed in our previous works [18,19] is the set of reactions of polyynes hydration followed by subsequent decomposition of the products to smaller hydrocarbons [11,12]. This provides the different behavior of polyynes, which concentration decreases by approximately one order of magnitude with increasing the number of carbon atoms in the polyynes molecules. The higher polyynes ($C_{10}H_2$ and $C_{12}H_2$) were excluded from the kinetic scheme because of the absence of thermodynamic data.

Soot precursors are formed by radical–molecule reactions of different PAHs starting from ace- and ethynynaphthalene up to coronene and radical–radical reactions (from cyclopentaphenanthrene up to coronene radicals). These reactions result in the formation of polyaromatic molecules containing from 24 to 48 carbon atoms,

which are stabilized by the formation of new chemical bonds. It should be noted that the C/H ratios of the soot precursors formed in these reactions are close to the upper boundary of the C–H diagram presented in [4]. Soot precursors are activated in reactions with H and OH radicals. They are deactivated in reactions with H, H₂, and H₂O. Soot precursors grow in reactions with C₂H₂, C₄H₂, and C₆H₂, whose concentrations are rather high in pyrolysis and oxidation of aliphatic and aromatic hydrocarbons, and in reactions with polyaromatic molecules and radicals, and in coagulation. Soot precursors are oxidized by O and OH radi-

cals. They are transformed into soot particles in the reactions of internal conversion, in which the number of active sites in the reacting system is preserved. Soot particles with active sites grow in the reactions with C₂H₂, C₄H₂, C₆H₂, and PAH molecules and radicals. All types of soot particles participate in coagulation. Oxidation of soot particles is described by reactions with O and OH radicals. Taking into account the experimental observations presented in [3,4,9,27], the polyynic submechanism of soot formation, introduced in the kinetic model formulated in [18] and further developed in [19], was excluded from the soot formation

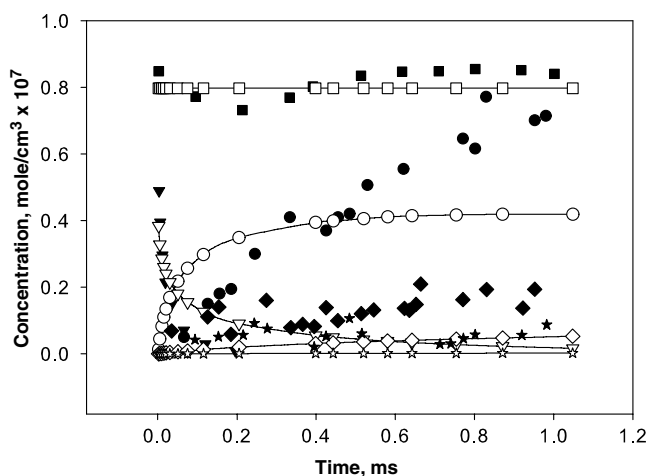


Fig. 1. Time dependences of the concentration of the main gas-phase species formed during pyrolysis of a 1.8% toluene mixture in neon at $T_5 = 1900$ K and $p_5 = 0.4$ bar behind reflected shock wave: (triangles down) toluene, (circles) C₂H₂, (diamonds) C₄H₂, (stars) C₆H₂, and (squares) $C_{\text{total}}/4$, where C_{total} is the total carbon atom concentration in the mixture. Open symbols and lines designate the results of our calculations, closed symbols the experimental measurements [20].

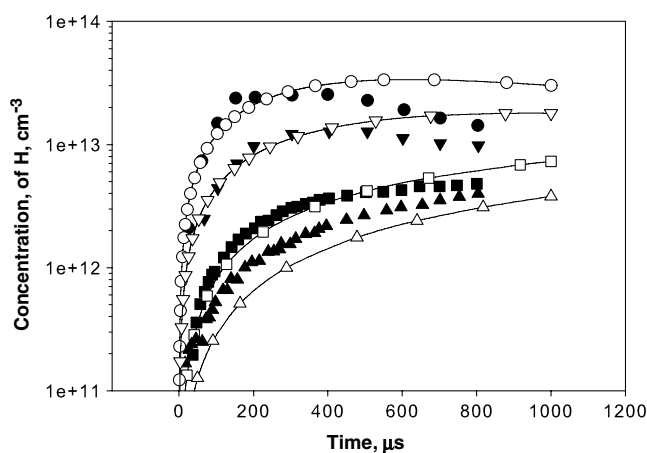


Fig. 2. Comparison of the experimentally measured (closed symbols) and calculated (open symbols) time dependences of H atom concentration during shock tube pyrolysis of benzene [21] and phenol [22]: (circles) $[C_6H_5OH]_0 = 20.5$ ppm in Ar, $T_5 = 1536$ K, $p_5 = 2.38$ bar, (triangles down) $[C_6H_5OH]_0 = 24.0$ ppm in Ar, $T_5 = 1477$ K, $p_5 = 2.06$ bar, (squares) $[C_6H_6]_0 = 1.8$ ppm in Ar, $T_5 = 1840$ K, $p_5 = 1.10$ bar, (triangles) $[C_6H_6]_0 = 3.2$ ppm in Ar, $T_5 = 1715$ K, $p_5 = 1.74$ bar.

model under consideration. An electronic copy of the mechanism and thermodynamic data is available from the authors (iz@chph.ras.ru or warnatz@iwr.uni-heidelberg.de).

3. Results and discussion

The results of calculations were compared with the experimental measurements of the main gas-phase species during shock tube pyrolysis of a tol-

uene/neon mixture [20]. As can be seen from Fig. 1, the kinetic model developed provides a rather good prediction of toluene consumption. A satisfactory description of the C_2H_2 , C_4H_2 and C_6H_2 concentration profiles are observed. The total balance of C atoms in the reacting mixture is predicted quite well. The reaction flow analysis shows that the major reactions of toluene consumption are $A1CH_2 + H = A1CH_3$ (43%), $A1CH_3 + H = A1CH_2 + H_2$ (41%), $A1CH_3 + H = A1 + CH_3$ (10%). The main channel of

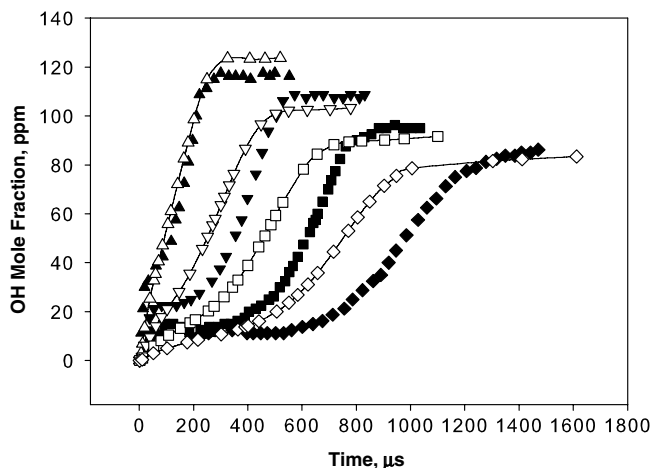


Fig. 3. Time dependences of the OH mole fraction obtained behind reflected shock waves: $\phi = 1$, 0.025% toluene + 0.225% O_2 , (triangles up) $T_5 = 1783$ K, $p_5 = 1.84$ bar, (triangles down) $T_5 = 1700$ K, $p_5 = 1.89$ bar, (squares) $T_5 = 1648$ K, $p_5 = 2.03$ bar, (diamonds) $T_5 = 1607$ K, $p_5 = 2.03$ bar. Open symbols and lines designate the results of our calculations, closed symbols the experimental measurements [23].

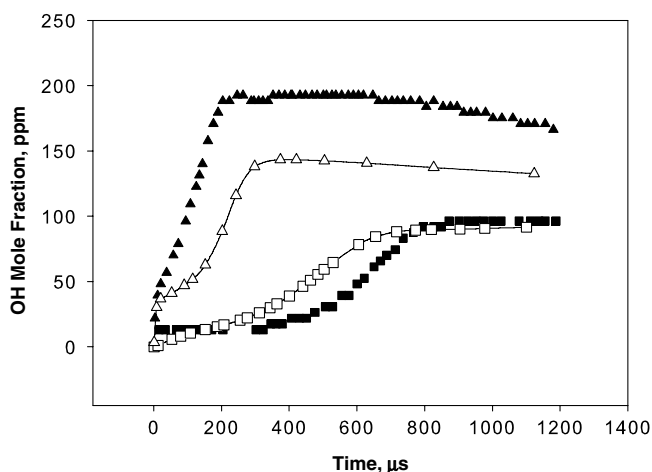


Fig. 4. Time dependences of the OH mole fraction obtained behind reflected shock waves for oxidation of *n*-heptane (*n*-alkane) and toluene (aromatic hydrocarbon): (triangles up) $\phi = 1$, *n*-heptane 300 ppm, *n*-heptane, $T_5 = 1640$ K, $p_5 = 2$ bar, (squares) $\phi = 1$, *n*-heptane 250 ppm, toluene, $T_5 = 1648$ K, $p_5 = 2$ bar. Open symbols and lines designate the results of our calculations, closed symbols the experimental measurements [23].

acetylene production is the decomposition of toluene radical (45%). The nomenclature used in the present work was the same as in [10–12].

The kinetic model considered was also tested to simulate the H concentration and OH mole fraction profiles recently measured in shock tube in [21–23]. Figures 2 and 3 demonstrate that the kinetic model predicts the H concentration and OH mole fraction profiles rather good at the relatively high temperatures and predicts the shorter ignition delay times at the lower temperatures. The reaction flow analysis demonstrates that during toluene oxidation OH radicals are formed mainly in the reactions $O + H_2 = H + OH$ (11%), $HO_2 + H = OH + OH$ (21%), $H + O_2 =$

$O + OH$ (51%) and are consumed in the reactions $OH + H_2 = H + H_2O$ (19%), $CO + OH = CO_2 + H$ (44%).

It is pertinent to note that the model predicts properly the different behavior of the OH mole fraction in *n*-heptane and toluene oxidation (Fig. 4). In *n*-heptane oxidation a quasistationary level of the OH concentration is attained at approximately 300 μs and in toluene oxidation at 800 μs under conditions presented in Fig. 4. This difference is caused by the different times, when the maximal concentration of CO is attained, which consumes OH radicals: 232.8 μs for *n*-heptane and 678.5 μs for toluene.

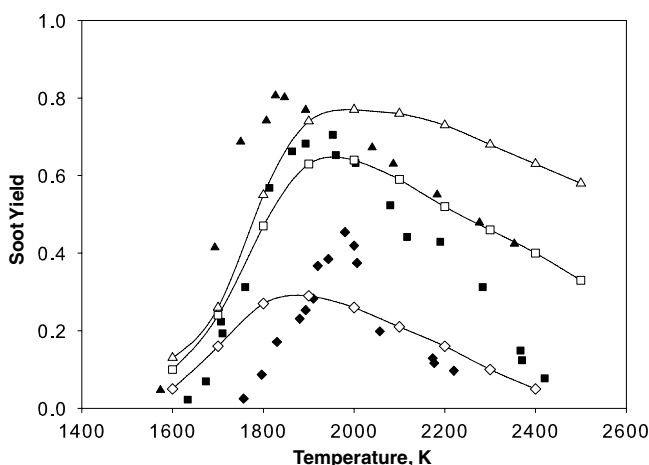


Fig. 5. Temperature dependences of the experimentally measured [24] (closed symbols) and calculated (open symbols) soot yield in the pyrolysis of argon diluted toluene mixtures for the reaction time $\tau_{\text{reac}} = 2$ ms: (triangles) 1.5% toluene, $p_5 = 3.5$ bar, (squares) 1.0% toluene, $p_5 = 3.3$ bar, (diamonds) 0.5% toluene, $p_5 = 2.5$ bar.

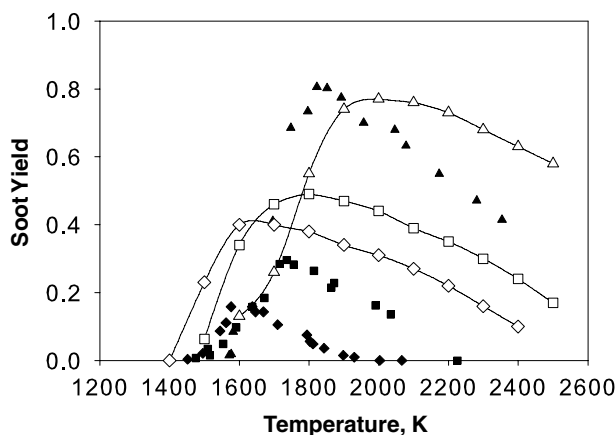


Fig. 6. Temperature dependences of the experimentally measured [24] (closed symbols) and calculated (open symbols) soot yield in the pyrolysis and oxidation of argon diluted toluene mixtures for the reaction time $\tau_{\text{reac}} = 2$ ms: (triangles up) 1.5% toluene, $p_5 = 3.5$ bar, (squares) 1.5% toluene + 1.5% O_2 , $p_5 = 2.0$ bar, (diamonds) 1.5% toluene + 2.5% O_2 , $p_5 = 2.0$ bar.

The results of calculations were compared with the experimental measurements performed in [24] for soot formation in pyrolysis of argon diluted toluene mixtures, binary toluene/methanol and toluene/ethanol mixtures, and for toluene oxidation behind reflected shock waves.

Figure 5 shows that the model provides a quantitative description of the temperature dependences of soot yield during pyrolysis of various argon diluted toluene mixtures. The soot yield increases with an increase in the initial toluene concentration, also with an increase in temperature reaching a maximum and later decreasing giving a typical bell-shaped distribution. The reaction flow analysis shows that soot precursors are formed mainly in reactions of acenaphthalene with acenaphthalene radicals and biphenyl molecules. Soot precursors are mainly activated in

reaction with H atoms and consumed in coagulation reactions. The main surface growth reactions are those with C_2H_2 (77%) and C_4H_2 (8%). Soot particles are also activated preferably in the reaction with H atoms and deactivated in the reactions with H and H_2 . Soot particle surface growth is provided by the reaction with C_2H_2 (97%). They are consumed in coagulation reactions (28%).

One can see from Fig. 5 that the model considered slightly underestimates the soot yield at the low temperatures and overestimates the soot yield at the high temperatures. In our opinion, together with the imperfections of the gas-phase mechanism and thermodynamic data, some restrictions in realization of the discrete Galerkin technique used for description of the heterogeneous reactions are responsible for these deviations.

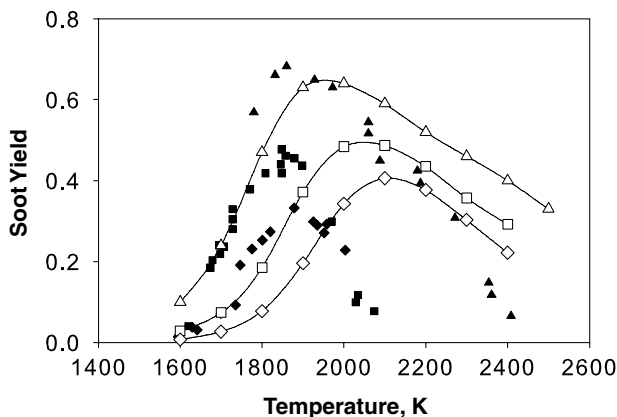


Fig. 7. Temperature dependences of the experimentally measured [24] (closed symbols) and calculated (open symbols) soot yield in the pyrolysis of argon diluted toluene and toluene/methanol mixtures for the reaction time $\tau_{\text{reac}} = 2$ ms: (triangles up) 1.0% toluene, $p_5 = 3.3$ bar, (squares) 1.0% toluene + 1.0% methanol, $p_5 = 2.7$ bar, (diamonds) 1.0% toluene + 2.0% methanol, $p_5 = 2.7$ bar.

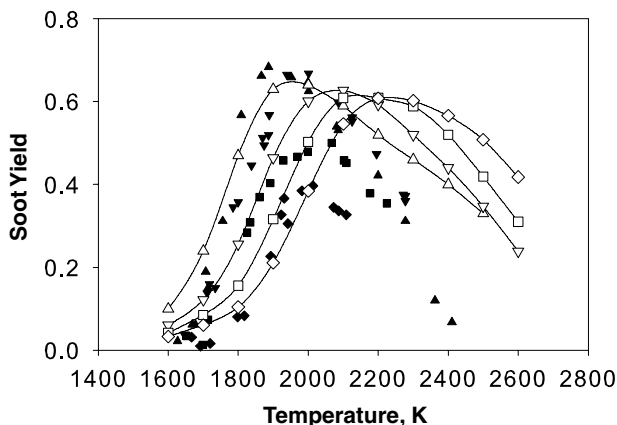


Fig. 8. Temperature dependences of the experimentally measured [24] (closed symbols) and calculated (open symbols) soot yield in the pyrolysis of argon diluted toluene and toluene/ethanol mixtures for the reaction time $\tau_{\text{reac}} = 2$ ms: (triangles up) 1.0% toluene, $p_5 = 3.3$ bar, (triangles down) 1.0% toluene + 1.0% ethanol, $p_5 = 3.0$ bar, (squares) 1.0% toluene + 2.0% ethanol, $p_5 = 3.0$ bar, (diamonds) 1.0% toluene + 3.0% ethanol, $p_5 = 3.0$ bar.

Oxygen addition to toluene not only suppresses soot formation but shifts the soot yield to lower temperatures as is shown in Fig. 6. The model considerably overestimates the soot yield in this case because the contribution of the surface oxidation reactions with the chosen rate coefficients is very small as compared with the contribution of the gas-phase oxidation reactions. The effect of methanol and ethanol addition to toluene is

demonstrated in Figs. 7 and 8, correspondingly. Both methanol and ethanol suppress soot formation at the lower temperatures although this reduction is only significant when the methanol exceeds 50% and the ethanol exceeds 70% of the total fuel mixture to be pyrolyzed. Thus, methanol suppresses soot formation slightly more effectively than ethanol. The maximum of the soot yield in the case of methanol and espe-

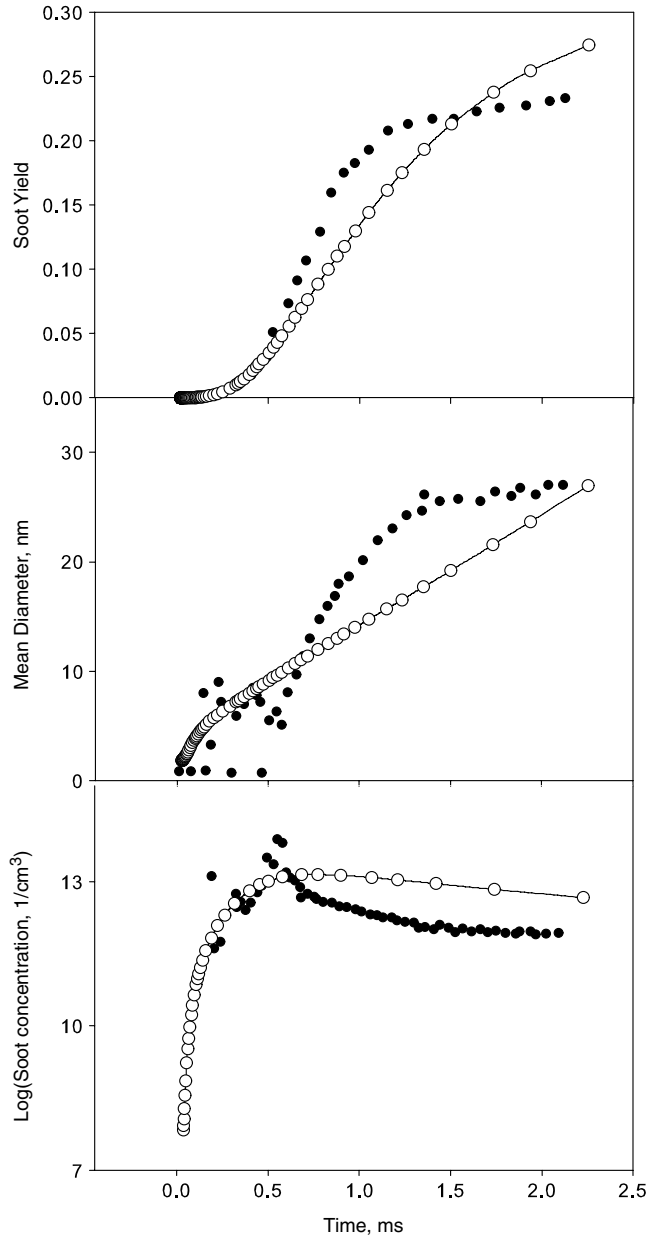


Fig. 9. Time dependences of the soot yield, the mean diameter of soot particles, and the logarithm of concentration of soot particles in the rich oxidation of the argon diluted *n*-heptane/O₂ mixture: $\varphi = 5$, $[C]_0 = 7.89 \text{ mol/m}^3$, $T_5 = 1750 \text{ K}$, $p_5 = 25 \text{ bar}$. Open symbols and lines designate the results of our calculations, closed symbols the experimental measurements [25].

cially ethanol addition is shifted to the higher temperatures (Figs. 7 and 8).

The results of calculations of the main parameters of soot formation for *n*-heptane oxidation were compared with the experimental measurements presented in [25] (Fig. 9). The reaction flow analysis demonstrates that *n*-heptane is consumed mainly in the reactions of decomposition with the formation hydrogen atom and various *n*-heptane radicals, in the reactions of *n*-heptane with H, OH, H₂ and H₂O, and in the reaction of *n*-heptane decomposition with the formation of C₄H₉ and C₃H₇. Acetylene is formed mainly in reactions of C₂H₃ decomposition (70%) and consumed in reactions of surface growth of soot particles, in the oxidation reactions with O and OH, and CH₂ radicals. First aromatic ring (benzene molecule) is formed mainly in the combination reaction of propargyl radicals (C₃H₃ + C₃H₃ = C₆H₆ (73%)) and preferably consumed in reactions with H atoms (C₆H₆ + H = C₆H₅ + H₂ (54%)). The main channel of soot precursor formation is reaction of acenaphthalene with acenaphthalene radical. They are activated mainly in reactions with H and deactivated by H and H₂. Surface growth occurs in reactions with C₂H₂ (91%) and C₄H₂ (2%). Soot particles are activated in reactions with H and deactivated by H, H₂, and H₂O. The main surface growth reaction is C₂H₂ addition (HACA). The main reactions of soot precursor and soot particle oxidation are similar to those observed in the case of toluene oxidation.

In Fig. 10, the temperature dependences of the experimentally measured [25] and calculated soot yield in rich oxidation of argon diluted *n*-heptane/O₂ mixtures are presented. The model predicts somewhat slower rates of soot growth during the period of active surface growth. The model slightly underestimates the soot yield at high temperatures but reproduces the dependence of the soot yield on the initial hydrocarbon concentration.

To gain more quantitative insight into the behavior of active sites on the surface of soot pre-

cursors and soot particles, the kinetic model was modified. In this case, the discrete index, utilized in the discrete Galerkin technique for calculation of the number of C atoms in particles [28], was used to determine the mean number of active sites per particle possessing of a particular mean diameter. This number increases in the reactions of activation and decreases in the reactions of deactivation and surface growth. For example, every reaction of surface growth results in the consumption of one active site, but the total number of active sites is preserved in coagulation reactions. The mean number of active sites per particle was related to the particle mean diameter determined in our previous calculations for the same reaction times. From this, the number density of active sites on the surface of soot particles was estimated and compared with the number density of C_{soot}-H sites (2.3×10^{15} sites/cm²) [5]. The calculations for toluene pyrolysis showed that for the temperature range of 2000–2300 K the mean number of active sites on the surface of soot particles, depending on the time and temperature, varies from several hundreds up to ten thousand, that is less than one order of magnitude in comparison to the total number of C_{soot}-H sites on their surface. In the case of *n*-heptane oxidation a considerable increase of the number of active sites is observed at *T* = 1700 K near the maximum of the soot yield.

4. Conclusions

The new detailed kinetic model of soot formation in shock tube pyrolysis and oxidation of aliphatic and aromatic hydrocarbons is proposed. The model is based on the comprehensive kinetic model of PAH formation and growth, which incorporates several pathways such as the alternative H-abstraction/C₂H₂-addition (HACA) route, resulting in a successive growth of PAHs, the combination reactions of phenyl with benzene molecules,

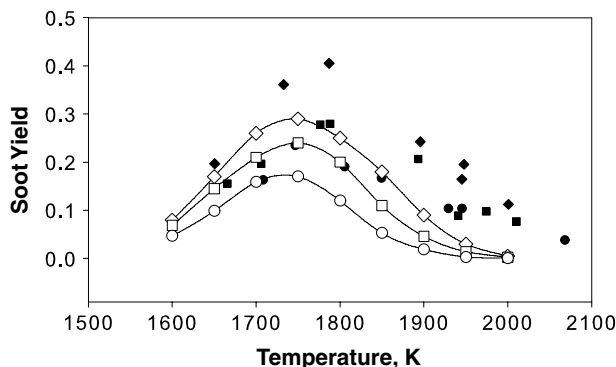


Fig. 10. Temperature dependences of the experimentally measured [25] (closed symbols) and calculated (open symbols) soot yield in the rich oxidation of the argon diluted *n*-heptane/O₂ mixture, $\phi = 5$, at constant Ar concentration of 99% for the reaction time $\tau_{\text{reac}} = 2$ ms: (diamonds) $p_5 = 50$ bar, (squares) $p_5 = 40$ bar, (circles) $p_5 = 30$ bar.

the cyclopentadienyl recombination, the ring closure reactions of aliphatic hydrocarbons, and the combination reactions of resonantly stabilized radicals. Soot precursors are formed in PAH molecule–radical and PAH radical–radical reactions. The new pathways of PAH formation introduced in the gas-phase kinetic mechanism and the new concepts of soot nucleation and the traditional surface HACA route implemented in the kinetic model made it possible to demonstrate a decisive role of PAHs in the soot inception process and the surface HACA pathway in the soot surface growth. The results of calculations are in good agreement with the results of the experimental measurements. The behavior of active sites on the surface of soot precursor and soot particles was investigated.

Acknowledgment

This work was supported by the Deutsche Forschungsgemeinschaft.

References

- [1] A. Violi, *Combust. Flame* 139 (2004) 279–287.
- [2] H. Wang, M. Frenklach, *Combust. Flame* 110 (1997) 173–221.
- [3] P. Weilmünster, A. Keller, K.-H. Homann, *Combust. Flame* 116 (1999) 62–83.
- [4] A. Keller, R. Kovacs, K.-H. Homann, *Phys. Chem. Chem. Phys.* 2 (2000) 1667–1675.
- [5] M. Frenklach, H. Wang, *Proc. Combust. Inst.* 23 (1990) 1559–1566.
- [6] M. Frenklach, *Phys. Chem. Chem. Phys.* 4 (2002) 2028–2037.
- [7] H. Richter, J.B. Howard, *Phys. Chem. Chem. Phys.* 4 (2002) 2038–2055.
- [8] H. Richter, S. Granata, W.H. Green, J.B. Howard, *Proc. Combust. Inst.* 30 (2005) 1397–1405.
- [9] Berk Öktem, M.P. Tolocka, B. Zhao, H. Wang, M.V. Johnston, *Combust. Flame* 142 (2005) 364–373.
- [10] J. Appel, H. Bockhorn, M. Frenklach, *Combust. Flame* 121 (2000) 122–136.
- [11] M. Frenklach, D.W. Clary, T. Yuan, W.C. Gardiner Jr., S.E. Stein, *Combust. Sci. Tech.* 50 (1986) 79–115.
- [12] M. Frenklach, J. Warnatz, *Combust. Sci. Tech.* 51 (1987) 265–283.
- [13] C. Correa, H. Niemann, B. Schramm, J. Warnatz, *Proc. Combust. Inst.* 28 (2000) 1607–1614.
- [14] M.S. Skjøth-Rasmussen, P. Glarborg, M. Østberg, J.T. Johannessen, H. Livbjerg, A.D. Jensen, T.S. Christensen, *Combust. Flame* 136 (2004) 91–128.
- [15] A. Violi, A.F. Sarofim, G.A. Voth, *Combust. Sci. Tech.* 176 (2004) 991–1005.
- [16] A. D'Alessio, A. D'Anna, P. Minutolo, L.A. Sgro, A. Violi, *Proc. Combust. Inst.* 28 (2000) 2547–2554.
- [17] A. D'Anna, A. Violi, A. D'Alessio, A.F. Sarofim, *Combust. Flame* 127 (2001) 1995–2003.
- [18] P.A. Vlasov, J. Warnatz, *Proc. Combust. Inst.* 29 (2002) 2335–2341.
- [19] I. Naydenova, M. Nullmeier, J. Warnatz, P.A. Vlasov, *Combust. Sci. Tech.* 176 (2004) 1667–1703.
- [20] R.D. Kern, H.J. Singh, M.A. Esslinger, P.W. Winkler, *Proc. Combust. Inst.* 19 (1982) 1351–1358.
- [21] S. Scherer, Untersuchung pyrolytischer Reaktionen des Rußvorläufermoleküls Propargyl im Stoßwellenrohr, Dissertation, Universität Stuttgart, Institut für Physikalische Chemie der Verbrennung des DLR in Stuttgart, 2001.
- [22] C. Horn, P. Frank, in: Proceedings of the 4th International Conference on Chemical Kinetics, NIST, July 14–18, 1997, Gaithersburg, MD, USA.
- [23] V. Vasudevan, D.F. Davidson, R.K. Hanson, *Proc. Combust. Inst.* 30 (2005) 1155–1163.
- [24] A. Alexiou, A. Williams, *Combust. Flame* 104 (1996) 51–65.
- [25] H. Kellerer, A. Müller, H.-J. Bauer, S. Wittig, *Combust. Sci. Tech.* 113–114 (1996) 67–80.
- [26] P. Deuflhard, M. Wulkow, *Impact Comput. Sci. Eng.* 1 (1989) 269–301.
- [27] H. Böhm, H. Jander, *Phys. Chem. Chem. Phys.* 1 (1999) 3775–3781.
- [28] J. Sojka, Simulation der Rußbildung unter homogenen Verbrennungsbedingungen, Dissertation, Interdisziplinäres Zentrum für Wissenschaftliches Rechnen, Ruprecht-Karls-Universität Heidelberg, 2001.

Comment

Med Colket, United Technologies Research Center, USA. In the pyrolysis of toluene, Colket and Seery [1] argued that the dominant reaction pathway to form naphthalene is a recombination reaction between C_7H_7 (benzyl) and propargyl (C_3H_3). Did you include this step? If not, why not?

Reference

- [1] M. Colket, D. Seery, *Proc. Combust. Inst.* 25 (1993) 883–891.

Reply. The reaction of benzyl (C_7H_7) and propargyl (C_3H_3) radical recombination described in the work of Colket and Seery was included in the model. This is the fastest reaction and gives the major amount of naphthalene in pyrolysis of toluene.